Colloquium: Miniature insect flight

Mao Sun*

Institute of Fluid Mechanics, Beihang University, Beijing 100191, China

(published 21 December 2023)

Many of the existing winged-insect species are extremely small (wing length ≈ 0.3–4 mm); they are referred to as miniature insects. Yet, until recently much of our knowledge about the mechanics of insect flight was derived from studies on relatively large insects, such as flies, honeybees, hawkmoths, and dragonflies. Because of their small size, many miniature insects fly at a Reynolds number (Re) on the order of 10 or less. At such a low Re, the viscous effect of the air is substantial: A miniature insect moves through the air as a bumblebee would move through mineral oil. The great importance of viscosity for miniature insects means that their flight relies on physical mechanisms that are different than those exploited by large insects. These differences range from the nature of the wing stroke to the structure of the wings, with some insects even using porous (bristled) wings to fly. Over the past decade, much work has been done in the study of the mechanics of flight in miniature insects: novel flapping modes have been discovered and new mechanisms of aerodynamic-force generation have been revealed; progress has also been made on fluid-mechanics-related flight problems such as flight power requirements and flight dynamic stability. This Colloquium reviews these developments and discusses potential future directions.

DOI: 10.1103/RevModPhys.95.041001

CONTENTS

I. INTRODUCTION

The size of winged insects varies greatly (Dudley, 2000). The insects that we see most often, for instance, flies, honeybees, hawkmoths, and dragonflies, are relatively large; their wing length (R) ranges from approximately 5 to 50 mm (Dudley, 2000). But many winged insects are extremely small, with R being approximately 0.3–4 mm (Polilov, 2015), and we rarely notice them. Here we call these small insects miniature insects, while we refer to the relatively large ones as medium and large insects. Figure 1 shows the significant difference in size between a typical miniature insect and a medium size insect: the small wasp *Encarsia formosa* could fit inside the eye of a drone fly. Close to half of the existing winged-insect species are of a miniature size (Dudley, 2000). Until recently most knowledge regarding the mechanics of flight of insects has been derived from studies on medium and large insects. For medium size insects, the relevant fluid flows have a Reynolds number Re on the order of hundreds, indicating that inertia is more important than viscous effects. However, the Reynolds number $\mathrm{Re} = \rho U c/\mu$, where ρ is the air density, U is the characteristic wing beating speed, c is the mean chord length of a wing, and μ is the air viscosity. Since both U and c decrease with insect size, Re is much smaller for miniature insects than for medium and large insects; for instance, $\mathrm{Re} \approx 10$ for the small wasp (Weis-Fogh, 1973). The great importance of viscosity for miniature insects means that their flight relies on physical mechanisms that differ from those exploited by medium and large insects. These differences range from the nature of the wing stroke to the structure of the wings, with some insects even using porous (bristled) wings to fly.

Before we discuss the flight of miniature insects, we provide an overview of the flight of medium and large insects; more detailed reviews were given by Sane (2003), Wang (2005), Shyy *et al.* (2010), and Shelley and Zhang (2011). Medium and large insects in hovering flight usually beat their wings back and forth in an approximately horizontal plane [Fig. 2(a)], actions referred to as upstroke and downstroke, respectively. The plane in which the wings beat is called the stroke plane (Weis-Fogh, 1973; Ellington, 1984c). Note that dragonflies use an inclined stroke plane [see Norberg (1975)] and that some insects, such as the hoverfly, use both horizontal and inclined stroke planes (Weis-Fogh, 1973). In the beginning of an upstroke or downstroke [Fig. 2(b)], the wing

*m.sun@buaa.edu.cn

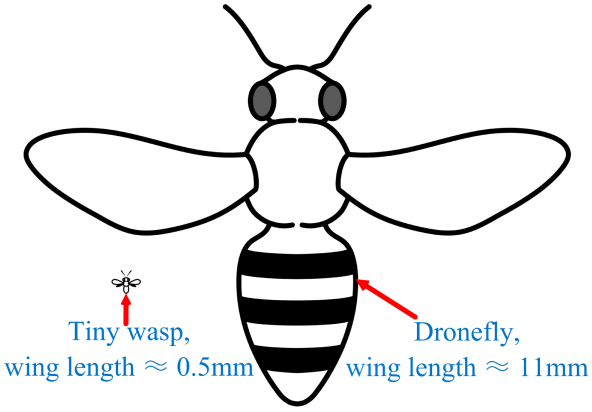

FIG. 1. Comparison between a typical miniature insect (a small wasp *Encarsia formosa*) and a medium size insect (a drone fly *Eristalis tenax*, which is the same size as a honeybee). Note that most of the smallest insects use bristled wings.

accelerates and pitches down at the same time; in the midportion of the stroke, the wing moves at an approximately constant speed [Fig. 2(b)]; near the end of the stroke, the wing decelerates and pitches up at the same time [Fig. 2(b)]. In forward flight, the stroke plane tilts forward (Dudley and Ellington, 1990a).

Although the wing of an insect beats at a high frequency (usually above 150 Hz), the velocity of the wing relative to the undisturbed air is small owing to the small wing length. As a result, the lift coefficient of the wing required to balance the weight is relatively high (Ellington, 1984a, 1984b, 1984c, 1984d); the mean lift coefficient required is around 2 (Liu and Kawachi, 1998; Sun and Du, 2003), which is about 3 times as large as that of a cruising airplane. This high lift coefficient cannot be explained by conventional steady-state aerodynamics and unsteady aerodynamic mechanisms must be operating (Ellington, 1984c). Several unsteady mechanisms have been proposed to explain the high aerodynamic-force coefficients. Among them are the "delayed-stall" mechanism (Ellington *et al.*, 1996), the "pitching-up rotation" mechanism (Dickinson, Lehman, and Sane, 1999; Sun and Tang, 2002a), and the "fast acceleration" mechanism (Sun and Tang, 2002a; Sane, 2003). The delayed-stall mechanism produces high lift by the leading-edge vortex (LEV), which attaches to and moves with the wing during an entire upstroke or downstroke. The fast acceleration mechanism is where a wing in fast acceleration at a large angle of attack can produce a large aerodynamic force. The "pitching-up rotation" mechanism is when a wing moves forward and at the same time pitches up quickly, and large lift and drag can be produced.

For many insects in hovering flight, it has been shown that the lift and drag of the wing generally have three peaks in an upstroke or downstroke (Wang, Birch, and Dickinson, 2004; Aono, Liang, and Liu, 2008; Liu and Sun, 2008), with an example shown in Fig. 3 (C_L and C_D are the lift and drag coefficients, respectively; t is the time and T is the flapping period; $t/T = 0$–0.5 is the upstroke and $t/T = 0.5$–1 is the downstroke). The force peak in the beginning of the upstroke ($t/T \approx 0$–0.1) or downstroke ($t/T \approx 0.5 - 0.6$) is produced by the fast acceleration mechanism. The "wider" force peak in the midportion of the upstroke ($t/T \approx 0.1$–0.4) or downstroke ($t/T \approx 0.6 - 0.9$) is due to the delayed-stall mechanism, i.e., due to the LEV attached to and moving with the wing [Fig. 3(c)]. The force peak near the end of the upstroke ($t/T \approx 0.4$–0.5) or downstroke ($t/T \approx 0.9$–1) is generated by the pitching-up rotation mechanism. Note that the force peak at the beginning of an upstroke or downstroke is much smaller than that in the midposition of the stroke. This is because although the wing is in fast acceleration, it is at the same time performing pitching-down rotation; see Fig. 2(b). The force

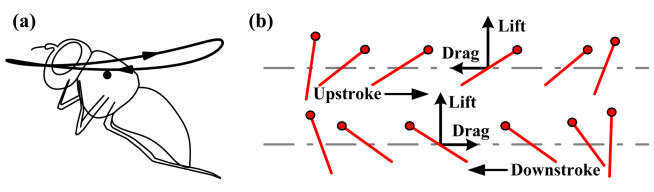

FIG. 2. (a) Stroke diagram showing the wing-tip trajectory (projected onto the symmetrical plane of the insect; the black curve) of the drone fly *Eristalis tenax*, a relatively large insect. A black dot defines the wing-root location on the insect body. (b) Motion of a section of the wing and definition of aerodynamic lift and drag, with dots marking the leading edge.

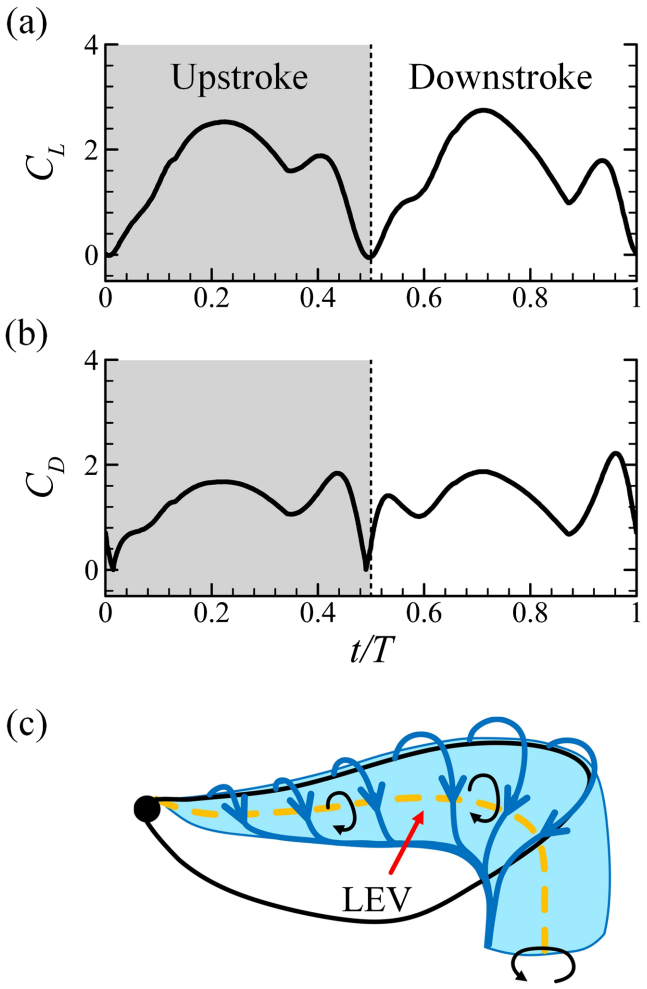

FIG. 3. (a) Lift and (b) drag coefficients of a drone fly in a flapping period. Adapted from Liu and Sun, 2008. (c) Sketch of the LEV on a flapping wing.

peak near the end of the upstroke and downstroke is also smaller; the reason for this is that, although the wing is in pitching-up rotation, it is also in fast deceleration.

The large lift peak in the midportion of the upstroke or downstroke, due to the delayed-stall mechanism, provides approximately 60%–70% of the stroke-cycle mean lift (Liu and Sun, 2008). We thus see that insects use the lift of the wings to provide the weight-supporting vertical force and that the high lift is produced mainly by the LEV that attaches to the wing.

The aforementioned results for medium and large insects, however, do not apply to the miniature insects, because of the large effect of air viscosity. As mentioned, Re decreases rapidly with decreasing insect size and for miniature insects such as the small wasp *Encarsia formosa*, Re is approximately 10. At such a low Re, the viscous effect of the air is so large that a miniature insect moves through the air as a bumble bee would move through mineral oil. The LEV would be significantly diffused owing to the large viscous effect, and little lift and a large drag are generated (Miller and Peskin, 2004; Lyu, Zhu, and Sun, 2019a). It was shown that at Re = 100–400 (Re of medium size insects) C_L and C_D are approximately 1.7 and 1.5, respectively, and the lift-to-drag ratio is approximately 1.3, while at Re = 10 C_L becomes only 0.9 and C_D reaches 3.1, and C_L/C_D is only 0.29 (Lyu, Zhu, and Sun, 2019a). Therefore, miniature insects must use different wing kinematics and aerodynamic mechanisms, even different wing structures (bristled wings), than medium and large insects use.

In the past ten years, much work has been done in the study of the mechanics of flight in miniature insects: novel flapping modes have been discovered and new mechanisms of aerodynamic-force generation have been revealed. Progress has also been made regarding fluid-mechanics-related flight problems such as flight power requirements and flight dynamic stability. In this Colloquium we review the significant work done thus far in the area of miniature insect flight and discuss potential future directions.

II. GOVERNING EQUATIONS

The governing equations of the flow around an insect are the incompressible Navier-Stokes equations,

$$\nabla \cdot \mathbf{u} = 0, \tag{1}$$

$$\frac{\partial \mathbf{u}}{\partial t} + \mathbf{u} \cdot \nabla \mathbf{u} = -\frac{1}{\rho}\nabla p + \nu \nabla^2 \mathbf{u}, \tag{2}$$

where $\boldsymbol{u}$ is the fluid velocity, p is the pressure, ρ is the density, ν is the kinematic viscosity, ∇ is the gradient operator, and ∇^2 is the Laplacian operator.

Using the wing chord length c as the reference length, the mean flapping speed U as the reference speed ($U = 2\Phi r_2 f$, where Φ is the flapping amplitude, r_2 is the radius of gyration of the wing area, and f is the flapping frequency), and c/U as the reference time, the nondimensionalized Navier-Stokes equations can be written as

$$\frac{\partial \boldsymbol{u}^*}{\partial t^*} + \boldsymbol{u}^* \cdot \nabla \boldsymbol{u}^* = -\nabla p^* + \frac{1}{\mathrm{Re}}\nabla^2 \boldsymbol{u}^*, \tag{3}$$

$$\nabla \boldsymbol{u}^* = 0 \tag{4}$$

where the asterisk represents a nondimensional quantity: $\boldsymbol{u}^* = \boldsymbol{u}/U$, $t^* = tU/c$, $p^* = p/\rho U^2$, and $\mathrm{Re} = cU/\nu$ (Reynolds number). If instead of c/U the flapping period T ($T = 1/f$) is used as the reference time, Eq. (3) becomes

$$\mathrm{St}\frac{\partial \boldsymbol{u}^*}{\partial t^*} + \boldsymbol{u}^* \cdot \nabla \boldsymbol{u}^* = -\nabla p^* + \frac{1}{\mathrm{Re}}\nabla^2 \boldsymbol{u}^*, \tag{5}$$

where $t^* = t/T$ and $\mathrm{St} = c/UT$ ($=cf/U$) (Strouhal number or reduced frequency).

It is well known that Re represents the ratio of the inertial force (the part of the inertial force caused by convection acceleration) to the viscous force of the fluid, and also that St represents the ratio of the characteristic time of body motion (here T) to the characteristic time of fluid convection (U/c). Since both U and T are related to the flapping frequency f, St can be written as $\mathrm{St} = c/\Phi r_2$. For many insects, Φ is approximately 120° and r_2/c is approximately 1.65 (Weis-Fogh, 1973). Hence, St ≈ 0.3. Re is proportional to both c and r_2. When an insect is small, both c and r_2 are also small, and Re will become low. That is, for a miniature insect the viscous-force term in Eq. (5) (the second term on the right) will be large, i.e., the viscous effect will be strong.

When the wing motion of an insect is given (usually by measurement), Eqs. (3) and (4) or Eqs. (5) and (4) can be numerically solved to give the flows around and the aerodynamic force acting on an insect. The equations are also used in the analysis of flows and aerodynamic mechanisms.

III. FLAPPING MODE CHANGE AND DIFFERENT AERODYNAMIC MECHANISMS

A. A typical miniature insect: *Encarsia formosa*

As mentioned in Sec. I, in order to generate the aerodynamic forces necessary for flight, miniature insects must have different flapping kinematics and aerodynamic mechanisms than medium and large insects have. What flapping pattern do the miniature insects use, and how do they generate the necessary aerodynamic forces? Cheng and Sun (2018) addressed these questions by studying the hovering flight of a typical miniature insect, the small wasp *Encarsia formosa*, which was brought to researchers' attention by the seminal work of Weis-Fogh (1973). Its wing length (R) is approximately 0.6 mm, its flapping frequency (f) is 360 Hz, and its mass (m) is about 0.02 mg. Cheng and Sun (2018) first used high-speed cameras to measure the detailed wing kinematics, and then, on the basis of the data, they solved the Navier-Stokes equations and obtained the flows around the insect and the aerodynamic forces acting on it.

They found that the miniature wasp has a distinctive pattern of wing motion. Figure 4 gives the wing-motion diagram. Let T be the period of the flapping cycle. A flapping cycle can be divided into four phases. To begin, in the upstroke the wings accelerate rapidly downward and backward at an almost 90°

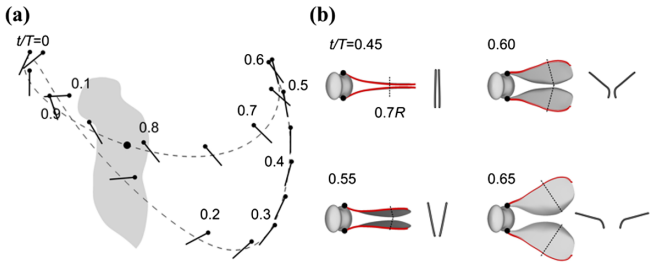

FIG. 4. (a) Stroke diagram showing the wing motion of *E. formosa*. The dashed curve indicates the wing-tip trajectory (projected onto the symmetrical plane of the insect); the black lines indicate the orientation of the wing at 20 temporally equidistant points, with dots marking the leading edge; and the black dot defines the wing-root location on the insect body. (b) Wing motion at dorsal stroke reversal showing the fling. R is the wing length. Adapted from Cheng and Sun, 2018.

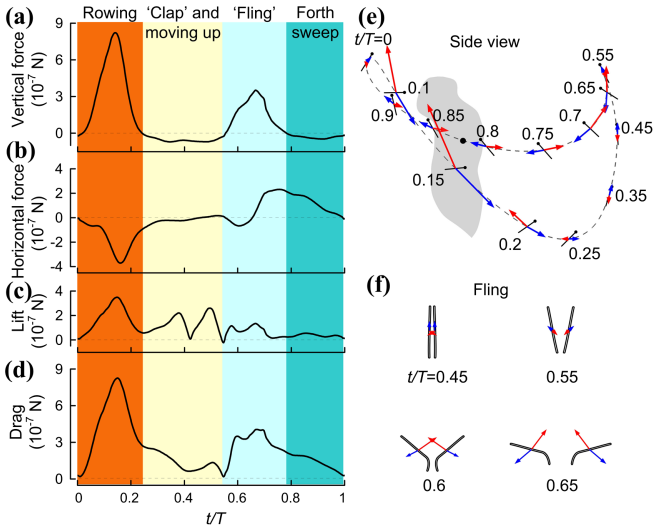

FIG. 5. Aerodynamic forces. (a)–(d) Vertical force, horizontal force, lift, and drag of a wing. (e) Diagram showing the wing position, velocity vector, and force vector at various times in one stroke cycle (side view). (f) Back view of the wing in fling motion, represented as the wing section at $0.7R$, and the corresponding velocity vector and force vector. Blue arrow, velocity; red arrow, force. Adapted from Cheng and Sun, 2018.

angle of attack [Fig. 4(a); $t/T \approx 0$–0.25 (the first phase)]. They then close up on the right and left sides on the back of the insect while moving slowly upward at an almost 0° angle of attack [Fig. 4(a); $t/T \approx 0.25$–0.5 (the second phase)]. At the beginning of the downstroke, the wings quickly rotate about their trailing edges [Fig. 4(b); $t/T \approx 0.5$–0.6 (the third phase)] and then sweep forward at a high angle of attack [Fig. 4(a); $t/T \approx 0.6$–1.0 (the fourth phase)]. The wing motion in the first phase, quickly accelerating downward and backward at almost a 90° angle of attack, resembles that of the stroking oars of a boat; this phase is referred to as impulsive rowing. The second phase is referred to as clap and slowly moving up. The third phase is the well-known "fling" motion, which was discovered in this species by Weihs and Barta (2008). The fourth phase is referred to as forward sweep. As mentioned in Sec. I, medium and large insects have planar upstrokes and downstrokes. For the small wasp, the upstroke has a deep U shape [Fig. 4(a)]. The downstroke also has a U shape, but it is much shallower. In an entire wingbeat cycle, the wing tip follows a twisted figure-eight loop [Fig. 4(a)].

What do these odd features of wing flapping provide in terms of aerodynamic-force production? The computed aerodynamic forces are shown in Fig. 5; in the figure and in the rest of this Colloquium, the vertical and horizontal components of the total aerodynamic force of a wing are referred to as the vertical force and the horizontal force, respectively. When the wing does not translate along the horizontal plane, the vertical force is not the lift of the wing and the horizontal force is not the drag of the wing. The velocity at the radius of gyration of the wing is used to represent the velocity of the wing [Fig. 5(e)]. Lift and drag are defined as the components of the total aerodynamic force that are perpendicular to and parallel to the velocity of the wing, respectively. As seen in Fig. 5, a large vertical-force peak is produced during the impulsive rowing [Fig. 5(a); $t/T \approx 0$–0.2], and another smaller one is generated during the fling and the beginning of the forward sweeping [Fig. 5(a); $t/T \approx 0.55$–0.75]. The other parts of the cycle do not produce any positive vertical force; during the "clap and slowly moving up" motion, the motion is slow and drag is small, and moreover two wings "clap" and move somewhat as one wing, further reducing their drag or the negative vertical force (Cheng and Sun, 2019). The impulsive rowing contributes 70% of the total vertical force, and the fling and the beginning of the forward sweeping contribute the other 30%.

Cheng and Sun (2019) further explained that the large vertical-force peak during the impulsive rowing is mainly from the drag of the wing, and that the large drag is due to the fast acceleration of the wing (referred to as the impulsive rowing mechanism). As for the vertical-force peak during the fling and the beginning of the forward sweeping, it is also mainly from the large drag of the wing [see Figs. 5(a), 5(d), and 5(f)]. The production mechanism of the large drag is where the opening of the wing pair generates a low-pressure region of rapidly swirling air that persists until the beginning of the forward sweeping, creating the large drag (referred to as the fling mechanism). The fling mechanism was discovered by Weis-Fogh (1973); it was further studied by many researchers including Miller and Peskin (2005) and Sun and Yu (2006).

We thus see that the small wasp uses the drag produced by distinctive wing motion and novel aerodynamic mechanisms (impulsive rowing and fling) to offset the otherwise formidable effects of increased viscosity. These two mechanisms can also be explained by examining the flow equations [Eq. (5)] and rewriting them as

$$\underbrace{\mathrm{St}\frac{\partial \boldsymbol{u}^*}{\partial t^*}}_{\substack{\text{inertial force}\\ \text{(local rate of change)}}} + \underbrace{\boldsymbol{u}^* \cdot \boldsymbol{\nabla} \boldsymbol{u}^*}_{\substack{\text{inertial force}\\ \text{(convection)}}} = -\boldsymbol{\nabla} p^* + \underbrace{\frac{1}{\mathrm{Re}} \boldsymbol{\nabla}^2 \boldsymbol{u}^*}_{\text{viscous force}}. \tag{6}$$

When Re is small, the viscous effect, represented as the second term on the right-hand side of Eq. (6), is large. As mentioned in Sec. II, the characteristic time used in St is usually T (flapping period). But when the wing has a large

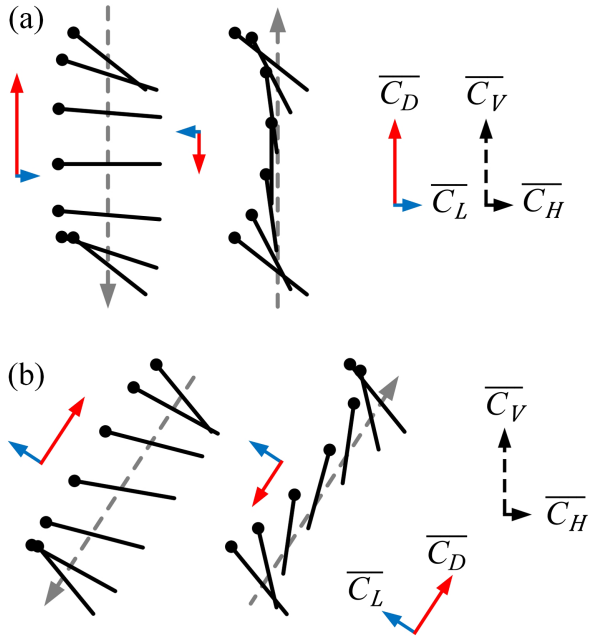

FIG. 6. Idealized wing kinematics (represented by a sections of the wing). The dot represents the leading edge of the wing, and the downstrokes and upstrokes are shown separately. The solid red arrows indicate the direction and relative magnitude of the dimensionless drag (C_D) during each downstroke or upstroke, and the solid blue arrows indicate the direction and relative magnitude of the dimensionless lift (C_L). The solid axes on the right indicate the net C_D and C_L during a flapping cycle. The directions of the dimensionless vertical (C_V) and dimensionless horizontal forces (C_H) always face the same way with respect to the global frame (the dashed arrows). (a) A vertical, drag-based stroke uses only C_D to produce C_V. (b) A tilted, hybrid stroke uses both C_L and C_D to produce C_V. Adapted from Jones *et al.*, 2015.

velocity change (i.e., large acceleration) in a short time, say, $0.1T$, there will be a new, smaller timescale. Using this smaller characteristic time as the reference time, St would be 1 order of magnitude larger. This would make the inertial force, the first term on the left-hand side of Eq. (6), large, thereby overcoming the large viscous effect.

That miniature insects may use the drag mechanism for flight was previously suggested (Horridge, 1956; Jones *et al.*, 2015). Two modes of wing motion that can use drag to produce weight-supporting vertical force (Fig. 6) were suggested by Jones *et al.* (2015). The downward motion of the wing in Fig. 6(a) looks similar to the rowing motion of the small wasp, but there is a major difference between the two: the discussion of the wing by Jones *et al.* (2015) suggested that motion moves at an approximately constant speed, while the real miniature insect moves with fast acceleration. Without large acceleration, the required large drag cannot be produced.

Using the downward motion of the wing (the first part of the U-shaped stoke) and drag to produce the vertical force has been shown in some insects. Wang (2004) found that for a hovering dragonfly (with an inclined stroke plane and asymmetric flapping) drag contributes approximately three-quarters of the required vertical force. Hovering hoverflies with an inclined stroke plane and asymmetric flapping use drag to support approximately three-quarters of the weight (Zhu and Sun, 2017). Dragonflies and hoverfies can also hover with a horizontal stroke plane (Ellington, 1984b); in this case the vertical force is produced using the lift principle only. That is, dragonflies and hoverflies can choose to use lift or drag to produce the required vertical force. However, the small wasps must use the downward wing motion and the drag principle to fly; moreover, rapid wing acceleration must be used.

B. Some miniature insects of different size

As mentioned, the upstrokes and downstrokes of medium and large insects are generally planar (Fig. 2). But for the small wasp *E. formosa* discussed in Sec. III, the planar upstroke commonly used by medium and large insects changes to a deep U-shaped upstroke [Fig. 4(a)]. The first part of the deep U-shaped upstroke (accelerating quickly downward) produces a large vertical force through the impulsive rowing mechanism, and the second part (wings clapped and slowly moving up) produces a small negative vertical force. Thus, the deep U-shaped upstroke gives a large mean vertical force and overcomes the otherwise formidable effects of increased viscosity.

The small wasp *E. formosa* is an extremely small insect: $R \approx 0.6$ mm and $\mathrm{Re} \approx 10$ ($m \approx 0.02$ mg). Lyu, Zhu, and Sun (2019a) examined the literature and noticed that small fruit flies, a relatively large miniature insect whose $R \approx 3$ mm and $\mathrm{Re} \approx 80$ ($m \approx 0.72$ mg), have a shallow U-shaped upstroke (Fry, Sayaman, and Dickinson, 2005). The wing-tip trajectory of the fruit fly compared with that of the small wasp is plotted in Fig. 7: the U upstroke of the fruit fly (at the top of Fig. 7) is much shallower than that of the small wasp (at the bottom of Fig. 7). This inspired Lyu, Zhu, and Sun (2019b) to conjecture that as the insect size decreases, i.e., Re decreases, deeper and deeper U-shaped upstrokes would be used to overcome the larger and larger viscous effects, as shown by the wing-tip trajectories drawn using dotted lines in Fig. 7.

Lyu, Zhu, and Sun (2019b) measured the wing motions of several insects with sizes smaller than that of the small fruit fly and larger than that of the small wasps. These insects are vegetable leaf miner *Liriomyza sativae* (LS) ($\mathrm{Re} \approx 40$, $R \approx 1.5$ mm, and $m \approx 0.25$ mg), biting midge *Forcipomia gloriose* (FG) ($\mathrm{Re} \approx 29.8$, $R \approx 1.4$ mm, and $m \approx 0.2$ mg), biting midge *Dasyhelea flaviventris* (DF) ($\mathrm{Re} \approx 23.7$, $R \approx 0.95$ mm, and $m \approx 0.08$ mg), gall midges *Anbremia sp.* (AS) ($\mathrm{Re} \approx 17.4$, $R \approx 1.3$ mm, and $m \approx 0.05$ mg), and thrips *Frankliniella occidentalis* (FO) ($\mathrm{Re} \approx 13.5$, $R \approx 0.79$ mm, and $m \approx 0.02$ mg). The stroke diagrams showing the flapping mode of the these insects are plotted in Fig. 8. As mentioned, medium and large insects such as the drone fly (Fig. 2) have an approximately planar upstroke and downstroke, while in Fig. 8 we see that for miniature insects, the upstroke changes to a U shape, and as size decreases deeper and deeper U-shaped upstrokes are employed [Figs. 8(a)–8(g)]. This is just what Lyu, Zhu, and Sun (2019b) conjectured; see Fig. 7.

Moreover, for the two smallest of these insects, thrips *F. occidentalis* and the small wasp *E. formosa*, the downstroke also becomes U shaped, but the downstroke U-shaped curve is shallower than that of the upstroke [Figs. 8(f) and 8(g)].

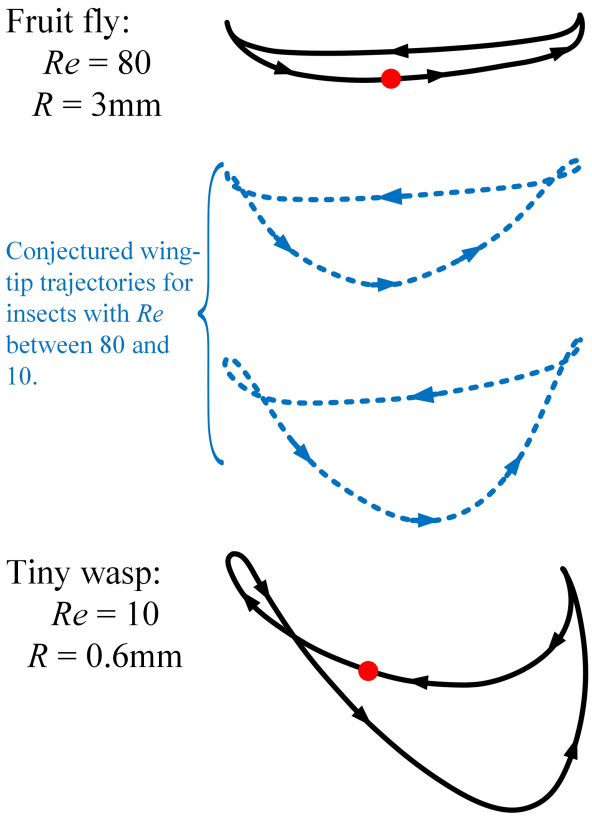

FIG. 7. Top diagram: wing-tip trajectory (projected onto the symmetrical plane of the insect) of a fruit fly ($R = 3$ mm), which is a relatively large miniature insect. Bottom diagram: wing-tip trajectory of a small wasp ($R = 0.5$ mm), which is a typical miniature insect. Middle diagrams: conjectured wing-tip trajectories for insects with sizes in between.

Thus, in an entire wingbeat cycle the wing tip follows a "twisted" figure-eight loop.

Using the wing-motion data, Lyu, Zhu, and Sun (2019b) solved the Navier-Stokes equations and obtained the aerodynamic forces acting on the insects, and they showed the following: For the relatively large miniature insects, the U-shaped upstroke produces a larger vertical force than planar upstroke by having a larger wing velocity. For the extremely small ones, like the small wasp *E. formosa* discussed in Sec. III.A, the U-shaped upstroke becomes deep, and in its first phase the wing smashes on the air (impulsive rowing) and generates a large drag directed upward (vertical force). On the contrary, in its second phase the wing slices slowly through the air and generates a small drag directed downward. They also showed that the fling mechanism was used by some of the miniature insects.

Note that the asymmetric stroke, which is "downward moving at a large angle of attack and upward moving at a near-zero angle of attack," is also used by some large insects (for instance, dragonflies and hoverflies); the downward motion provides a large vertical force for weight support and the upward motion ("slicing the fluid") produces only a small downward force (Sun and Lan, 2004; Wang, 2004). The difference is that the downward wing motion of miniature insects has an impulsive start that increases the magnitude of the drag or vertical force in a viscous flow.

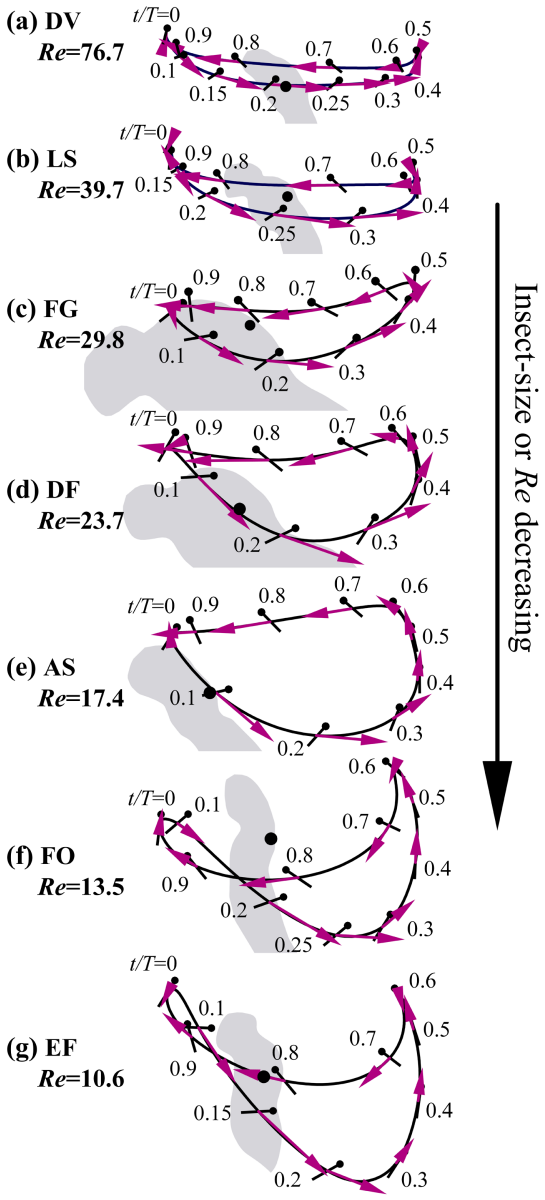

FIG. 8. Stroke diagrams showing the wing motions of the insects. The solid curve indicates the wing-tip trajectory (projected onto the symmetrical plane of the insect); black lines indicate the orientation of the wing at various times in one stroke cycle, with dots marking the leading edge; a black dot defines the wing-root location on the insect body; and the purple arrow represents the velocity of the wing at the radius of gyration. Adapted from Lyu, Zhu, and Sun, 2019b.

C. An even smaller miniature insect (a small beetle with bristled wings)

In Sec. III.B, the flight of some miniature insects of different size were discussed, with the smallest ones being the small wasp *E. formosa* and the thrips *F. occidentalis* ($m \approx 0.02$ mg). But there are many even smaller winged insects. Most of these smallest winged insects have bristled wings (Polilov, 2005; Farisenkov *et al.*, 2020); a bristled wing is sketched in Fig. 9.

Do these even smaller insects use an even deeper U-shaped upstroke, use both a deep U-shaped upstroke and a deep

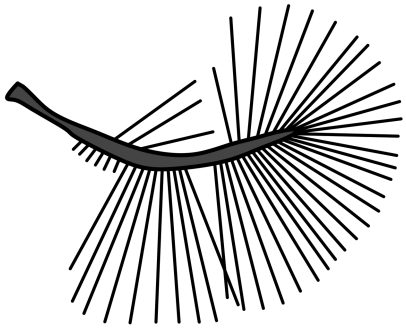

FIG. 9. Sketch of the bristled wing of a small beetle *Paratuposa placentis* plotted according to the photograph taken by Farisenkov *et al.* (2022).

U-shaped downstroke, or use another novel flapping mode? Recently Farisenkov *et al.* (2022) studied the flight of the small beetle *Paratuposa placentis*. Its m is only 0.0024 mg, $R = 0.49$ mm, $f = 180$ Hz, and $\mathrm{Re} = 9$ (for *Encarsia formosa*, which was discussed in Sec. III.A, $m = 0.02$ mg, $R = 0.6$ mm, and $f = 360$ Hz; in comparison, the small beetle *P. placentis*, m of *E. formosa* is 8.3 times as large and R is only 22% larger, but f is twice as high). They used high-speed videography to obtain the wing kinematics, electron microscopy measurements to obtain the morphological data, and computational fluid mechanics methodology to compute the flow and aerodynamic forces.

The measured wing kinematics is shown in Fig. 10 by a diagram of wing-tip trajectory (side view) and a wing orientation at 20 points of the equal time interval. In Fig. 10, curve *ABC* is the wing-tip trajectory of the upstroke and curve *CDA* is that of the downstroke. An upstroke (or downstroke) can be divided into two phases, called the power phase and the recovery phase, respectively, by Farisenkov *et al.* (2022).

We first look at the upstroke. In the first phase (the power phase) of the stroke (Fig. 10, from *A* to *B*), the wings move downward and backward at large velocity and acceleration at nearly a 90° angle of attack. In the second phase (the recovery phase) of the upstroke (Fig. 10, from *B* to *C*), the wings move upward slowly at nearly a zero angle of attack [at the beginning of the moving up, the two wings close up (clap) at the back of the insect (this can be seen in Fig. 11)], and near the end of the moving up the wings start to separate from each other. Note that the upstroke of the small beetle is similar to the deep U-shaped upstroke of the previously discussed small insects. Next we look at the downstroke. In the first phase of the stroke (Fig. 10, from *C* to *D*), as in the first part of the upstroke, the wings move at large velocity and acceleration at nearly a 90° angle of attack, but here they move downward and forward, not downward and backward. In the second phase of the stroke (Fig. 10, from *D* to *A*), as in the case of the upstroke, the wings move upward slowly at nearly a zero angle of attack; the two wings are also closed, but now the wings are in front of the insect. The downstroke is also similar to a deep U-shaped stroke. Since both the upstroke and the downstroke are a deep U shape, the wing-tip trajectory is a figure-eight loop (Fig. 10).

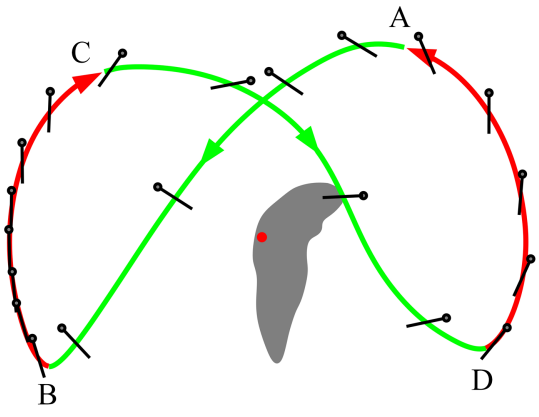

FIG. 10. Stroke diagrams showing the wing motions of *Paratuposa placentis*. The solid curve indicates the wing-tip trajectory (projected onto the symmetrical plane of the insect); black lines indicate the orientation of the wing at various times in one stroke cycle, with dots marking the leading edge; a red dot defines the wing-root location on the insect body. Adapted from Farisenkov *et al.*, 2022.

On the basis of the measured kinematic and morphological data, Farisenkov *et al.* (2022) computed the flow around the insect and obtained the aerodynamic force on the bristled wings. As seen in Fig. 11, large, nearly upward pointing drag is produced by the wing in the first phase of the U-shaped upstroke, when the wings move at large velocity and acceleration at nearly a 90° angle of attack (the impulsive rowing mechanism), and small, nearly upward pointing drag is produced in the second phase, in which the wings move upward slowly. This is also the case for the downstroke (Fig. 11).

The smallest insects discussed in Secs. III.A and III.B), i.e., the small wasp *E. formosa* and thrips *F. occidentalis*, mainly

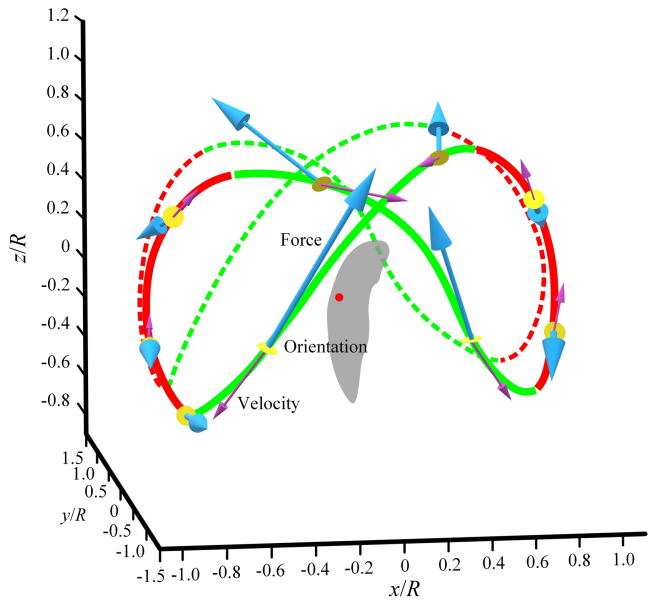

FIG. 11. Wing-tip trajectories and direction of aerodynamic force and wing velocity. Cyan arrows show aerodynamic force, magenta arrows show wing-tip velocity, and yellow disks show dorsal surface orientation of the wing at nine time instants. Opaque and transparent curves correspond to the right and left wings, respectively. Adapted from Farisenkov *et al.*, 2022.

use a deep U-shaped upstroke (impulsive rowing mechanism) and a shallower U-shaped downstroke to overcome the strong viscous effect. The small beetle *P. placentis* discussed here is even smaller. From the previous discussion, we see that the wing-motion style of the small beetle *P. placentis* is only slightly different from that of the thrips *F. occidentalis* and the small wasp *E. formosa*. Comparing Fig. 8(f) and 8(g) with Fig. 10, it is seen that they all have a deep U-shaped upstroke; the only difference is that the small beetle *P. placentis* also has a deep U-shaped downstroke, while the thrips *F. occidentalis* and the small wasp *E. formosa* have only a shallower U-shaped downstroke. For the thrips *F. occidentalis* and the small wasp *E. formosa*, in an entire wingbeat cycle the wing tip follows a twisted figure-eight loop [Figs. 8(f) and 8(g)], while for the small beetle *P. placentis* the wing tip follows a "normal" figure-eight loop (Fig. 10).

In Sec. III, we have discussed eight species of miniature insects whose wing kinematics have thus far been measured. The size of these insects, represented by body mass m, ranges from $m \approx 0.72$ mg (the small fruit fly *D. virilis*) to $m \approx 0.0024$ mg (the small beetle *P. placentis*). From the measured data (Figs. 8 and 10), the following trend regarding flapping pattern variation is observed: The planar upstroke commonly used by the medium and large insects changes to a U-shaped upstroke; as the size of the insect becomes smaller, deeper and deeper U-shaped upstrokes are used. When m decreases to about 0.02 mg (the small wasp *E. formosa* and thrips *F. occidentalis*), the downstroke also becomes U shaped, but the U shape is shallower [Figs. 8(f) and 8(g)]. When m decreases to about 0.0024 mg (small beetle *P. placentis*), the downstroke also becomes deep U shaped (Fig. 10). The features of a deep U-shaped upstroke or downstroke are as follows: In its first phase [wings quickly accelerating downward and backward (or forward)], a large vertical force is produced by the impulsive rowing mechanism. In its second phase (wings clapped and slowly moving up), only a small negative vertical force is produced. Thus, the deep U-shaped upstroke or downstroke gives a large mean vertical force.

IV. BRISTLED WINGS ENHANCE THE FLIGHT EFFICINCY OF EXTREMELY SMALL INSECTS

Many of the smallest flying insects have bristled wings (Fig. 9), for instance, thrips (Lewis, 1973), small beetles (Polilov, 2005), and fairy flies (Huber and Noyes, 2013). Some of them, such as the small wasp *E. formosa*, have partially bristled wings (Weis-Fogh, 1973).

The wing surface area of a bristled wing is much smaller than that of the membranous wing of the same outline. Therefore, it has been commonly considered that a bristled wing is much lighter than the equivalent membranous wing, and hence the inertial power for flapping a bristled wing would be much less than that for the membranous wing; see Sunada *et al.* (2002) and Weihs and Barta (2008). However, formal quantitative studies on this possible merit have only recently been conducted (Farisenkov *et al.*, 2022; Jiang *et al.*, 2022). In their study of the small beetle *P. placentis*, Farisenkov *et al.* (2022) determined the mass and moment of inertia of the bristled wing on the basis of the measured data. They estimated the mass and moment of inertia of the equivalent membranous wing using the wing thickness of some of the smallest membranous-winged insects (body length of about 0.8 mm). They found that the bristled wings are lighter than the equivalent membranous wings and have a much smaller moment of inertia. With the moment of inertia of the bristled and membranous wing evaluated, they numerically solved the Navier-Stokes equations and computed the inertial and aerodynamic powers of the free-flying small beetle (the power required for flight is the sum of the aerodynamic and inertial power; see Sec. VI). They found that with the bristled wing the instantaneous power may reach up to 110 W per kilogram of body mass ($\mathrm{W\,kg^{-1}}$) in the power phase of the flapping cycle, while with the membranous wings the value can reach up to 180–210 $\mathrm{W\,kg^{-1}}$ because of the large inertial power due to the large moment of inertia. With the bristled wing, the time-averaged power is 28 W per kilogram of body mass (the value is approximately the same with or without elastic energy storage since the wing is light). But with a membranous wing, even with perfect elastic energy storage the time-averaged power reaches 37 W per kilogram of body mass. The bristled wing makes the elastic energy storage obsolete and greatly reduces the peak mechanical power requirements of the flight muscles.

As discussed, the projected wing area of a bristled wing is much smaller than that of the equivalent membranous wing; for example, the projected wing area of the bristled wing of the miniature beetle *P. placentis* is only 15% that of the equivalent membranous wing (Kolomenskiy *et al.*, 2020). This means that the force per unit area of a bristled wing is much larger than that of the corresponding membranous wing. Furthermore, the bristles are slender and seem to be flexible. One might intuitively wonder whether the bristles would have large deformation and whether the wing geometry could be maintained.

Jiang *et al.* (2022) recently investigated this problem. They considered the bristled wings of the parasitoid wasp *Anagrus Haliday*. They first measured the morphological characteristics and the Young's modulus of the bristles. Next they performed fluid-structure-interaction computations [i.e., they solved the Navier-Stokes equations (3) and (4) coupled with the equilibrium equation for elastic body] of a model bristled wing. Their measurements showed that the bristles have a conical tubular structure, tapering toward the tip, and that the Young's modulus of the bristles is in the range of 18.6–25.2 GPa, which is much higher than that conventionally considered value for bristles (8–10 GPa) (Seale *et al.*, 2018). Their computations showed that at the extreme flow velocity and angle of attack (90°) of small wasps given in literature, the bristles deflect only marginally (a bending angle of less than 0.3°). That is, the bristled wing at high aerodynamic loading has negligible deformation and wing geometry could be maintained.

The aforementioned results are for the parasitoid wasp *A. Haliday*. No such detailed quantitative studies have yet been conducted for any other miniature insects. However, in high-speed video recordings of several free-flying miniature insects with bristled wings, for instance, thrips in takeoff flight (Santhanakrishnan *et al.*, 2014) and hovering flight (Lyu, Zhu, and Sun, 2019b), the small wasp *E. formosa* in hovering

(Weis-Fogh, 1973; Cheng and Sun, 2018), and the small beetle *P. placentis* in hovering and forward flight (Farisenkov *et al.*, 2022), no noticeable wing (bristles) deformation has been observed. This indicates that the slender bristles have special morphological structure and material characteristics for resisting deformations.

The aforementioned results (Farisenkov *et al.*, 2022; Jiang *et al.*, 2022) show that the flight weight of the bristled wing (greatly reducing inertial power) and the sophisticated design of the bristle structure (extremely stiff and leading to a marginal deformation) enable the flapping flight in the smallest insects. This is an important discovery in this area of study.

V. FORCE-PRODUCTION MECHANISMS AND SOME OTHER MERITS OF BRISTLED WINGS

As discussed in Sec. IV, for many of the extremely small insects a bristled wing is a prerequisite for their efficient flapping flight. Therefore, it is of interest to engage in further discussion of the aerodynamic mechanisms of bristled wings and the advantages of a bristled wing over a membranous wing.

A. Aerodynamic force

Sunada *et al.* (2002) measured the aerodynamic forces on a model bristled wing and a solid-plate wing of the same shape. Different simple wing motions were considered: azimuthally rotating at a constant angular speed and at a constant angular acceleration and translating at a constant speed and a constant acceleration. They showed that while flying at Re of around 10 or below, the aerodynamic forces acting on the model bristled wing were only a little smaller than those on the solid-plate wing [miniature insects with bristled wings fly at Re $\approx$ 10 or below (Sunada *et al.*, 2002; Lyu, Zhu, and Sun, 2019b; Farisenkov *et al.*, 2022)]. In the aforementioned experiments (Sunada *et al.*, 2002), the wing model has a rectangular planform and the bristles are in the chordwise direction. In a real bristled wing (as sketched in Fig. 9), in the inner part of the wing the bristles point forward and backward, while in the outer part of the wing the bristles point laterally. Kolomenskiy *et al.* (2020) performed experimental and numerical studies using a model bristled wing of realistic morphology of a miniature beetle. They found that, in the considered biologically relevant regimes of flow parameters, the bristled wing produced between 60% and 96% of the aerodynamic force of an equivalent membranous wing. In the experiment, the wing performed constant-speed rotation, not real flapping motion. In some recent numerical studies, realistic wing motions, a realistic bristled-wing morphology of a small beetle (Farisenkov *et al.*, 2022), and a small wasp (Jiang *et al.*, 2022) were used. It was shown that the bristled wing produced an aerodynamic force that is more than 80% that of the corresponding membranous wing.

The aforementioned studies show that, at Re of the bristled-winged miniature insects (Re $\approx$ 10 and below), the bristled wing can produce aerodynamic forces that are only slightly smaller than the corresponding membranous wing.

B. Production mechanisms of aerodynamic force

A bristled wing is morphologically much different than a membranous wing of the same outline. The membranous wing is solid, like a flat plate, while the bristled wing has gaps between the bristles, like a comb (Fig. 9). The gap width is approximately 10 times the bristle diameter (Sunada *et al.*, 2002; Jones *et al.*, 2016). Their aerodynamic-force production mechanisms should be different. As discussed in Sec. III, the wings of the smallest insects move at nearly a 90° angle of attack, producing large drag to provide the weight-supporting vertical force. For a flat-plate wing moving at nearly a 90° angle of attack, the drag comes mainly from the pressure difference between the windward and the rearward surfaces of the wing (frictional force is tangential to the surfaces and makes only a slight contribution to the drag). For a bristled wing, the situation is different. Each bristle of the wing is a slender "cylinder." When the Reynolds number of the wing is 10 (based on the mean chord length of the wing), the Reynolds number of the bristle is only about 0.05 (based on the diameter of the bristle). That is, the flows around the bristles must be Stokes flows and the drag on the bristles must be similar to that of a cylinder in the Stokes flow, half of the contribution from the friction force and half from the pressure force. Cheer and Koehl (1987) examined the flows and drag of a model bristled wing represented by a pair of cylinders, using the existing analytical solution of the Oseen equation obtained from matched-asymptotic analysis (Umemura, 1982). Barta and Weihs (2006) modeled the bristled wing by a row of parallel slender bodies (rodlike ellipsoids with a slenderness ratio smaller than 0.01) and solved the Stokes equation analytically. In these models, the bristles generate forces by the Stokes-flow (or the creeping-flow) mechanism. Since they solved the Stokes or Oseen equation, the Reynolds number of their model wing (Re based on wing chord length) needs to tend to zero, i.e., Re $\ll$ 1. The flow near the "bristle" (the near field) and the flows in the far field are all Stokes flows. Lee, Lee, and Kim (2020) and Wu, Liu, and Sun (2021) modeled the bristled wing using a row of two-dimensional circular cylinders and solved the Navier-Stokes equation numerically. Here Re can be any value, as long as it is low enough for turbulence to not occur (for miniature insects, Re $\approx$ 10; this is not a problem). Lee, Lee, and Kim (2020) considered the effects of varying the gap width between bristles and varying Re on the flows around the bristles. Wu, Liu, and Sun (2021) investigated the effects of wing acceleration. Both group's results showed the following: When Re of the bristled wing is about 10 or less (the Reynolds number of a bristle is about 0.05 or less), the flow near each bristle is Stokes flow in nature. The streamlines in the front of the bristle and those in the back are symmetrical; the surface frictional force and pressure force have approximately the same contribution to the drag on the bristle. The flow away from the bristles (the far field) resembles that of the corresponding flat-plate wing. Recently Jiang *et al.* (2022) used a realistic configuration of the bristled wings of a small wasp and realistic flapping motion in their numerical solution of the Navier-Stokes equations. They also found that approximately half of the contribution of the aerodynamic force on the bristle comes

from the surface pressure force and half comes from the surface friction force.

From the aforementioned results, we see that the drag production mechanism of the bristled wing is different than that of the membranous wing. For the membranous wing, the flow is blocked by the wing, giving a positive pressure on the windward surface and a negative pressure on the leeward surface; the drag is due to the pressure forces and the frictional stress makes almost no contribution. For the bristled wing, each bristle operates in a creeping flow and produces thick and strong shear layers; strong viscous force generates a large pressure difference between the windward and leeward surfaces of each bristle and large frictional stress on the bristle surface, resulting in a large drag on each bristle, and pressure and frictional forces make equal contributions to the drag.

C. Other merits of the bristled wings

As seen in Sec. V.A, a bristled wing operating at Re of the order of 10 or less could produce an aerodynamic force close to that of a membranous wing. And it has been shown that the light weight of bristled wings makes the efficient flight of the extremely small insect possible (Sec. IV). The bristled wing also has some other merits; an example is given later.

Some bristled-wing miniature insects perform the fling motion at the beginning of the downstroke [in the fling motion, the left and right wings are initially parallel and close to each other (i.e., they are clapped) and the wings then rotate quickly around the trailing edge and open to form a V shape]; see Weis-Fogh (1973). In the later stage of the fling motion, a relatively large vertical force can be produced; this aerodynamic-force production mechanism is referred to as the fling mechanism (Maxworthy, 1979). The fling motion can also enhance the vertical-force production in the subsequent downstroke; see Cheng and Sun (2021). The fling motion was identified in the small wasp *E. formosa* in 1973 (Weis-Fogh, 1973), and since then many studies were based on this motion (Miller and Peskin, 2005, 2009; Arora *et al.*, 2014). Membranous wings were considered in these studies: the flow structure and aerodynamic-force production mechanism, the effects of the initial distance between the two wings, the effects of wing flexibility, etc., were studied. One of the important results of these studies is that the cost of flinging is rather high: the drag required to "open" the wings apart may be an order of magnitude large than the force require to move a single wing with the same motion. Is it like this for bristled wings? Santhanakrishnan *et al.* (2014) investigated this question using two-dimensional (2D) porous flat plates to simulate the bristled wings. They numerically solved the Navier-Stokes equations for the porous plates and the corresponding solid plates. They found that, compared to solid wings, the porous nature of the wings contributes largely to drag reduction. This result may indicate that bristled wings, compared to solid wings, reduce the drag required to fling the two wings apart. However, a porous plate is not a bristled wing; it was desired to study the flows of bristled wings directly. Jones *et al.* (2016) studied the flows and aerodynamic forces of 2D bristled wings and the corresponding solid wings by numerically solving the Navier-Stokes equations. Kasoju and Santhanakrishnan (2021) studied the case of three-dimensional (3D) wings experimentally, using robotic bristled-wing models. Both the 2D numerical study and the 3D experimental studies showed that, in fling motion, bristled wings significantly decrease the drag required to fling the wings apart compared to the case of solid wings.

VI. POWER REQUIREMENTS AND FLIGHT STABILITY: SIZE EFFECTS

A. Power requirements

The wings of a flying insect must produce vertical force to support its weight and thrust to propel its body moving through the air. When producing these forces, the flight muscles must do work to move the wings against the aerodynamic drag and accelerate the wing mass. The power needed to overcome the aerodynamic force is referred to as the aerodynamic power, and that required to overcome the wing's inertial force is referred to as the inertial power. The sum of these two is the mechanical power that the flight muscles must deliver. When the metabolic rate of the flight muscles is known, the mechanical power can give the mechanochemical efficiency of the muscles, and knowing how much contribution the inertial power makes to the mechanical power can tell us whether or not an elastic muscle system is essential for insects (Ellington, 1984c; Dudley and Ellington, 1990b). Therefore, the study of the mechanical power requirement is of great importance for understanding the physiological and biomechanical mechanisms of insect flight.

The calculation of the inertial power is relatively simple. When the flapping kinematics and the wing mass and its distribution are measured, the wing's rotational velocity and acceleration and the moments of inertia of the wing can be obtained. From these data, the inertial power can be straightforwardly computed by means of a calculation of the aerodynamic power involving flow computation, i.e., numerically solving the Navier-Stokes equations [Eqs. (3) and (4)], or a force and moment measurement using a dynamically scaled wing model. Conventionally the mechanical power is denoted by P and its flapping-cycle-mean value denoted by $\bar{P}$. Because the wings have acceleration in some parts of the cycle and deceleration in other parts, the inertial power, and hence the mechanical power P, may become negative in some parts of the cycle. How the negative power fits into the power budget depends on the elastic energy storage of the flight muscle. When calculating $\bar{P}$, researchers commonly consider two limiting cases, and the real $\bar{P}$ lies between these limits (Dudley, 2000). One limiting case is 0% elastic energy storage, in which the negative work is ignored in the power budget; the other limiting case is 100% elastic energy storage, in which the negative mechanical work can be completely stored in an elastic element and later released to do positive work. The cycle-mean mechanical power divided by the mass of the insect is referred to as the mass-specific power, denoted as P^*,

$$P^* = \bar{P}/m, \tag{7}$$

where m is the mass of the insect. Note that P^* represents the power required per unit mass (weight) of the insect. Since $\bar{P}$ has

two limiting values, so does P^*. In the case of 0% elastic power storage, the mass-specific power is denoted as $(P^*)_1$; in the case of 100% elastic power storage, it is denoted as $(P^*)_2$.

Earlier studies on flight power requirements were for medium and large insects, for which the wing's kinematic and morphological data were available (Dudley and Ellington, 1990a; Sun and Tang, 2002b; Young *et al.*, 2009). In recent years, the required data have been measured for a number of miniature insects (Lyu, Zhu, and Sun, 2019b; Farisenkov *et al.*, 2022), and their power requirements can be computed. Lyu and Sun (2021) calculated the power requirement of six species of miniature insects in hovering flight; these insects are vegetable leaf miners LS ($m \approx 0.25$ mg), biting midges FG ($m \approx 0.2$ mg), biting midges DF ($m \approx 0.08$ mg), gall midges AS ($m \approx 0.05$ mg), thrips FO ($m \approx 0.02$ mg), and small wasps *E. formosa* ($m \approx 0.02$ mg). The masses of these miniature insects range from 0.02 to 0.25 mg. From the literature, they obtained the power requirement data for medium and large insects with masses ranging from about 1 (fruit fly *D. melanogaster*) to 1600 mg (hawkmoth *Manduca sexta*). With the power requirements of the miniature insects and those of the medium and large insects available, they could examine how the power requirement changed with size across the "full size range" of insects. Figure 12, which was adapted from Lyu and Sun (2021), compares the mass-specific powers of the insects [the nine species of medium and large insects considered in the earlier literature and the six species of miniature insects considered by Lyu and Sun (2021)]. More recently Farisenkov *et al.* (2022) computed the power requirement of an even smaller miniature insect, the small beetle *P. placentis* ($m \approx 0.0024$ mg), and their results $(P^*)_1 \approx (P^*)_2 = 28\ \mathrm{W\,kg^{-1}}$ are also added to Fig. 12. Note that in the computations of Lyu and Sun (2021) one species of small insects (thrips *F. occidentalis*) have bristled wings, but the wings were modeled by an equivalent membranous wing. In the computation of Farisenkov *et al.* (2022), for the small beetle *P. placentis* a realistic bristled-wing model was used.

In Fig. 12, the mass of the smallest insect (the small beetle *P. placentis*) is 0.0024 mg and that of the largest insect (hawkmoth *M. sexta*) is 1648 mg. There is a 6 orders of magnitude difference in mass. As seen from Fig. 12, even with the large difference in size, these insects have a relatively small difference in their mass-specific power: $(P^*)_2$ of these insects approximately vary in the range of 20–40 W/kg, and $(P^*)_1$ vary in the range of 20–60 W/kg. Compared with the difference in their sizes, the difference in their mass-specific power is negligible; i.e., the power consumption of an insect in hovering flight is approximately proportional to its mass. Assuming that the mean power per unit of muscle mass is the same under the same type of muscle, the aforementioned size–specific-power relation indicates that the ratio of flight-muscle mass to insect mass is approximately the same for differently sized insects.

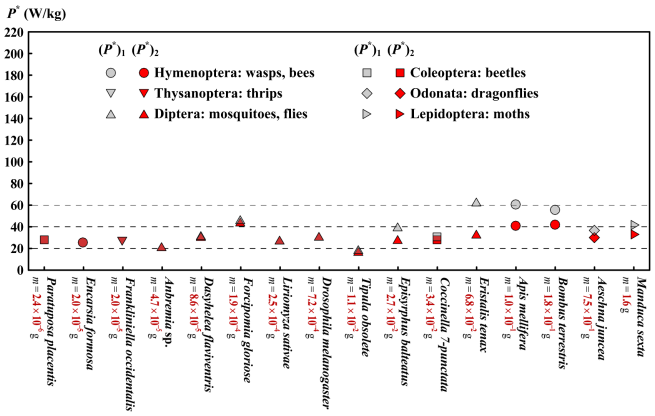

FIG. 12. Mass-specific powers in cases of 0% and 100% elastic energy storage for 16 species of insects. Adapted from Lyu and Sun, 2021.

The aforementioned results on miniature insects and medium and larger insects (Lyu and Sun, 2021) were obtained using the rigid-wing model. Insect wings are not rigid, and during flapping motion they deform and display small deviations from the rigid plane. Young *et al.* (2009) measured the wing deformation of a tethered locust in a wind tunnel, and based on the measured data they conducted a computational study on the effects of deformation. Their results showed that the power economy in locust flight can be improved by wing deformation. Walker, Thomas, and Taylor (2010) measured the wing deformation of freely flying hoverflies, and Du and Sun (2010) investigated the effect of wing deformation on aerodynamic forces using the data of Walker, Thomas, and Taylor (2010). It was shown that deformation increased the lift by about 10%, increased drag by about 3%, and decreased the aerodynamic power required to generate the lift by about 5% compared to the results for the rigid flat-plate wing. A 10% increase in lift, allied with a 5% reduction in aerodynamic power to generate that lift, could significantly enhance flight performance. Nakata and Liu (2012a) developed a fluid-structure-interaction (FSI) model of insect flapping flight with flexible wings. Using this FSI-based model, they performed a systematic analysis on the aerodynamic performance of a hovering hawkmoth (Nakata and Liu, 2012b). They showed that wing flexibility increased downwash in the wake and hence the aerodynamic force. Moreover, an increase in hovering efficiency of the flexible wing was achieved as a result of the wing twist. Ishihara (2018) and Cai *et al.* (2022) showed that using a model wing with three torsional springs at the wing hinge can satisfactorily determine the flexible wing behavior and its aerodynamic performance. Their model also showed that wing flexibility reduces the energy requirements of insect flight. These results of aerodynamic force and power expenditure with flexible wings are for medium and large insects (bumblebees, hawkmoths, and locusts), and also for flapping wing micro air vehicles (Hao, Wu and Zhang, 2019). For miniature insects, work on wind flexibility effects has not yet been done and should be considered for future study.

B. Flight stability

Dynamic flight stability (inherent or passive stability) is of great importance in the study of biomechanics of insect flight (Taylor and Thomas, 2003; Sun and Xiong, 2005; Cheng and Deng, 2011; Ristroph *et al.*, 2013). It is the basis for studying flight control because the passive stability of a flying system represents the dynamic properties of the basic system, such as

which degrees of freedom are unstable, how fast the instability develops, which variables are observable, etc.

In the study of flight stability in insects, the averaged model is commonly used (Taylor and Thomas, 2003): the insect is treated as a rigid body of 6 degrees of freedom and the action of the flapping wings is represented by the wingbeat-cycle-average forces and moments. Thus, the equations of motion of the insect are the same as those of an airplane. The equations of motion are linearized by approximating the body's motion as a series of small disturbances from a steady, symmetric reference flight condition. As a result of the linearization, the longitudinal and lateral small disturbance equations are decoupled and can be separately solved. The longitudinal (or lateral) small disturbance equations are a system of four linear differential equations. We denote the system matrix of the longitudinal (or lateral) equations as $\boldsymbol{A}$ (the values of the elements of $\boldsymbol{A}$ can be computed by numerically solving the Navier-Stokes equations or experimentally measuring the aerodynamic forces and moments of the flapping wings). The central elements of the solutions for the flight stability problem are the eigenvalues of $\boldsymbol{A}$. Being a fourth order matrix, $\boldsymbol{A}$ has four eigenvalues $(\lambda_1, \lambda_2, \lambda_3, \lambda_4)$. A real eigenvalue (or a conjugate pair of complex eigenvalues) represents a natural mode of the system. The motion of the flying body after an initial deviation from its reference flight is a linear combination of the natural modes. In a natural mode, the real part of the eigenvalue determines the time rate of growth of the disturbance quantities. A positive (negative) real eigenvalue will result in exponential growth (decade) of each of the disturbance quantities, so the corresponding natural mode is dynamically unstable [called the unstable divergent (stable subsidence) mode]. For an unstable divergent mode, the time to double the starting value (t_d) is given by

$$t_d = 0.693/\lambda \tag{8}$$

A pair of complex conjugate eigenvalues, for instance, $\lambda_{1,2} = s \pm \omega i$, will result in an oscillatory time variation of the disturbance quantities with ω as its angular frequency. The motion grows when s is positive (called the unstable oscillatory mode). The time to double the oscillatory amplitude is

$$t_d = 0.693/\mathrm{s}. \tag{9}$$

Until recently studies on flight stability addressed medium and large insects (Taylor and Thomas, 2003; Cheng and Deng, 2011; Wu and Sun, 2012); the masses of these insects range from about 1600 (hawkmoths) to about 1 mg (mosquitoes and fruit flies). This covers the mass range of many winged insects, except that of miniature insects, whose mass is more than 1 order of magnitude smaller. One reason for the absence of the stability analysis of miniature insects was that their wing kinematical and morphological data were not available. Recently the wing data for some miniature insects were measured (Lyu, Zhu, and Sun, 2019b; Farisenkov *et al.*, 2022), and the stability properties of these miniature insects can be calculated. As a first step, Lyu and Sun (2022) considered the longitudinal flight stability problem of two hovering miniature insects: the vegetable leaf miner *L. sativae* ($m \approx 0.25$ mg) and gall midge *Anbremia sp.* ($m \approx 0.05$ mg). They found that for each of the two miniature insects there is a pair of complex eigenvalues λ_1 and λ_2 that have a positive real part, and there are two negative real eigenvalues (λ_3 and λ_4), one with a large magnitude and the other with a small magnitude. Therefore, the longitudinal motion has three natural modes: an unstable oscillatory mode, a stable fast subsidence mode, and a stable slow subsidence mode. Owing to the unstable mode, the longitudinal motions of the gall midge and the vegetable leaf miner are unstable.

By comparing it to the results of the medium and large insects (Sun and Xiong, 2005; Cheng and Deng, 2011), they pointed out that the modal structure of the two miniature insects is the same as that of the medium and larger insects, having an unstable oscillatory mode, a stable fast subsidence mode, and a stable slow subsidence mode. That is, although the insects considered have a 30 000-fold difference in mass (mass of the gall midge, 0.05 mg; that of the hawkmoth, 16 000 mg), they have the same modal structure. Because of the unstable mode, the hovering flight of insects of all considered sizes is passively unstable. This means that flight must be actively controlled to be stable: the insects need to constantly react to their surroundings and adjust their wing motion in order to keep from tumbling. The response time of the nervous system needs to be fast enough to react and keep the unstable mode from growing too large. Therefore, the growth rate of the unstable mode is of much interest. The time to double the initial values of disturbances t_d [Eq. (7) or (8)] represents the growth rate of instability. Lyu and Sun (2022) calculated the values of t_d of the two miniature insects, and they also calculated the values of t_d for the other medium and larger insects using the values of λ_1 and λ_2 from previous studies. The value of t_d for the insects (12 species) are plotted in Fig. 13. An approximate analytical expression of t_d as a function of m was derived by Lyu and Sun (2022); it showed that t_d is proportional to the 0.17 power of m (also plotted in Fig. 13). That is, as m becomes smaller, t_d decreases (i.e., the instability becomes faster). This means that miniature insects need a faster nervous system to control instability than larger insects. For example, the response time, represented by t_d, of the miniature insect the gall midge ($m \approx 0.05$ mg) needs to be faster by approximately 7 times than that of the large insect the hawkmoth ($m \approx 1600$ mg).

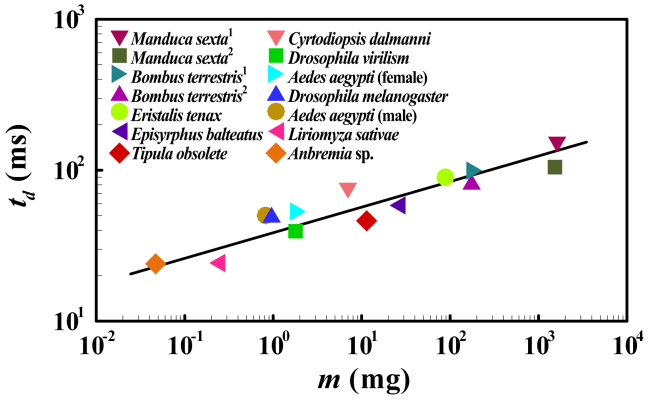

FIG. 13. Relationship between t_d and m of 12 species of insects. Adapted from Lyu and Sun, 2022.

The aforementioned results on flight stability were obtained by applying the averaged model. As discussed, the averaged model is based on assumptions about the rigid body, the rigid wing, the wingbeat-averaged forces and moments, and the wingbeat-averaged position of center of mass. Bluman, Sridhar, and Kang (2018) modified the averaged model by including wing flexibility. They showed that wing flexibility could influence the stability properties. However, their study considered only the effects of chordwise flexibility in a two-dimensional flow velocity field, and the resulting wing deformation gave a negative wing camber (experimental observations of flying insects showed that the deforming wings have a positive camber). Richter and Patil (2010) developed an integrated model of the flight dynamics and wing flexibility of a flapping wing (fruit-fly wing). Their model showed that the flight system is unstable, that the flexibility effects amplify a given stability or instability of the system, and that the flexibility effects reduce the damping of the present oscillatory mode. At present, for medium and large insects, work on the flexibility effect on flight stability is still limited; for miniature insects, work in this area has not yet been done.

In a recent study, Taha *et al.* (2020) argued that the direct averaging used in the averaged model might miss the stabilizing effect due to body oscillation. Their study concluded that for large insects such as hawkmoths flight was stable, which was the opposite of the results of the averaged model (the averaged model shows that flight is unstable). Their result indicating that body oscillation stabilizes flight is somewhat questionable; this is explained as follows: Gao, Aono, and Liu (2011) and Liang and Sun (2013) coupled the equations of 6-degree-of-freedom motion with the Navier-Stokes equations to study the flight stability of insects (including the large insect the hawkmoth). They showed that flight was unstable. This model fully included the body oscillation effect, but flight was unstable. Therefore, the issue of "body oscillation stabilizing flight" needs further examination.

VII. CONCLUDING REMARKS

To overcome the large viscosity effects, miniature insects must employ wing motion and aerodynamic mechanisms that differ from those of medium and large insects. Current data show the following changes: The planar upstroke commonly used by medium and large insects changes to a U-shaped upstroke. As the insect size (represented by its mass m) becomes smaller, deeper and deeper U-shaped upstrokes are employed. When m decreases to about 0.02 mg, the downstroke also becomes U shaped, but the U shape is shallower. When m decreases to about 0.0024 mg, the downstroke also becomes deep U shaped. The features of a deep U-shaped upstroke or downstroke are as follows: in its first phase the wings rapidly accelerate downward at nearly a 90° angle of attack, "smashing" the air and producing a large drag or vertical force (the impulsive rowing mechanism). On the contrary, in its second phase the wings are close to each other and move slowly upward at a zero angle of attack, "slicing" through the air and producing a small negative vertical force. Thus, the deep U-shaped upstroke or downstroke gives a large mean vertical force. Note that the aforementioned results were obtained from only eight species of insects, whose wing kinematics have previously been measured (fruit fly *D. virilis*, $m \approx 0.72$ mg; vegetable leaf miner *L. sativae*, 0.25 mg; biting midge *F. gloriose*, 0.2 mg; biting midge *D. flaviventris*, 0.08 mg; gall midge *Anbremia sp.*, 0.05 mg; thrips *F. occidentalis*, 0.02 mg; small wasp *E. formosa*, 0.02 mg; and small beetle *P. placentis*, 0.0024 mg). It is of much importance to measure the wing motion of more miniature insects to see whether the aforementioned trend of variations in flapping pattern is general, and whether there are other novel flapping patterns and new aerodynamic mechanisms.

The wings of many miniature insects are bristled rather than membranous. Thus far the numerical studies on bristled wings have been based on the Navier-Stokes equations with the no-slip condition on the bristle surface; experimental studies have used dynamically scaled models moving in mineral oil. That is, in both numerical and experimental studies, the flow is assumed to be in the continuum regime. It is known that, for the flow to be in the continuum regime, the Knudsen number (Kn) needs to be small [Kn is the ratio of the molecular mean free path of the air (λ) to a characteristic length of the geometry (L_c), for instance, the diameter of a cylinder]. Conventionally when $\mathrm{Kn} \lesssim 0.001$, the flow is well within the continuum regime, the Navier-Stokes equations are valid, and the no-slip boundary condition can be used. When $\mathrm{Kn} \gtrsim 0.001$, there are rarefied-gas effects on the flow, but if $0.001 \lesssim \mathrm{Kn} \lesssim 0.1$, the rarefied-gas effects mainly appear in the areas near the body boundary and the major phenomenon is that the no-slip condition is violated: the flow slips on the boundary (the flow regime of $0.001 \lesssim \mathrm{Kn} \lesssim 0.1$ is referred to as the slip regime). As noted by Liu and Aona (2009), because of the small geometrical length scales of the bristled wings, Kn may be larger than 0.001 and there may be rarefaction effects. At 20 °C and standard pressure, λ of the air is calculated as 0.065 μm. The diameter of the bristles (D) of the bristled wings, for which measurements have been made, ranges from about 0.6 to 2.0 μm (Jones *et al.*, 2016; Farisenkov *et al.*, 2022; Jiang *et al.*, 2022). Using D as the characteristic length, Kn ranges from 0.03 to 0.11; the flow is well within the slip regime and the rarefaction effects need to be studied. Recently a study on this problem was conducted (Liu and Sun, 2023) that showed that the rarefaction has only a small effect on the aerodynamic force of the bristled wing: it decreases the aerodynamic force by less than 0.5% that of the continuum flow. However, the rarefaction has a significant effect on the contributions of the viscous tangential and normal stress terms to the aerodynamic force: in the continuum flow, the force contribution of the viscous tangential stress is 50.7% and that of the viscous normal stress is zero, whereas in the slip flow, for instance, at $\mathrm{Kn} = 0.08$, the contribution of the viscous tangential stress is only 37.7% and that of the viscous normal stress is 12.9% instead of zero. This is only a preliminary study: the bristled wing was simplified to a row of two-dimensional cylinders and only steady-state motion was considered. More realistic geometry of the wing and fast acceleration motion of the wing should be considered in future research.

Dynamic flight stability analysis has been made for two species of miniature insects in hovering flight, the vegetable leaf miner *L. sativae* ($m \approx 0.25$ mg) and the gall midge

Anbremia sp. ($m \approx 0.05$ mg). The analysis showed that the longitudinal modal structure of the two miniature insects is the same as that of the medium and large insects: there is an unstable oscillatory mode, a stable fast subsidence mode, and a stable slow subsidence mode. The flight is unstable because of the unstable mode. The difference between a smaller insect and a larger one is that the instability of the smaller insect grows faster than that of the larger one. The stability analysis has been based on the averaged-model theory and treats the flight as a fixed-point equilibrium. Because of the periodically varying aerodynamic and inertial forces of the flapping wings, a hovering or constant-speed flying insect is a cyclically forcing system, and generally the flight is not in a fixed-point equilibrium but rather a cyclic-motion equilibrium. The averaged-model theory gives good results for insects with relatively small body oscillations at wingbeat frequency, but for some insects with relatively large body oscillations at wingbeat frequency (such as large moths and butterflies) cyclic-motion stability analysis is required (Wu and Sun, 2012). The wing and body motions of eight species of miniature insects have been video recorded and measured (Lyu, Zhu, and Sun, 2019b; Farisenkov *et al.*, 2022). From the video recordings, it can be observed that body pitch oscillation is large for the smallest insect of the eight species, the small beetle *P. placentis*: The body pitch angle variation in the oscillation is approximately 30°. For a miniature insect like this, one may need to treat the flight as a cyclic-motion equilibrium and use the Floquet theory or numerical simulation by solving the complete equations of motion coupled with the Navier-Stokes equations to analyze the flight stability. This is interesting and important future work (because knowing the passive stability properties of an insect is the basis for studying its stabilization of flight). Moreover, in most studies on the flight stability of insects (large or small), a rigid-wing model has been used; how wing flexibility (i.e., wing deformation) affects the stability properties needs to be studied.

Flight control is an important part of insect flight; without control, insects cannot really fly. Flight control involves coupling of the "inner" control systems (sensory system and neuron-motor control system) and the "outer" dynamics (passive stability, wing-motion change, and aerodynamic-force change). There are two broad types of flight control. One is stabilization control, which is used to stabilize flight (keep the disturbances from growing during hovering or constant-speed flight). The other is maneuver control, which is used to generate aerobatics, such as fast changing flight direction, recovering from upside-down falling, and landing on a ceiling. For medium and large insects, important studies have been made on both stabilization control (Ristroph *et al.*, 2010, 2013; Cheng, Deng, and Hedrick, 2011; Windsor, Bomphrey, and Taylor, 2014) and maneuver control (Haselsteiner, Gilbert, and Wang, 2014; Wang, Melfi, Jr., and Leonardo, 2022). For miniature insects, however, study on flight control is currently absent. Research in this direction is strongly recommended.

ACKNOWLEDGMENTS

M. S. thanks W. Y. Cai, X. Cheng, L. G. Liu, W. J. Liu, Y. Z. Lyu, and Z. H. Zhu, for their help, and D. Du, Y. P. Liu, and Y. l. Zhang for the useful comments. M. S. acknowledges financial support from the National Natural Science Foundation of China through Grants No. 11832004 and No. 11721202.

REFERENCES

Aono, H., F. Liang, and H. Liu, 2008, "Near- and far- field aerodynamics in insect hovering flight: and integrated computational study," J. Exp. Biol. **211**, 239.

Arora, N., A. Gupta, S. Sanghi, H. Aono, and W. Shyy, 2014, "Lift-drag and flow structures associated with the 'clap and fling' motion," Phys. Fluids **26**, 071906.

Barta, E., and D. Weihs, 2006, "Creeping flow around a finite row of slender bodies in close proximity," J. Fluid Mech. **551**, 1.

Bluman, J. E., M. K. Sridhar, and C. k. Kang, 2018 "Chordwise wing flexibility may passively stabilize hovering insects," J. R. Soc. Interface **15**: 20180409.

Cai, X. F., Y. J. Xue, D. Kolomenskiy, R. Xu, and H. Liu, 2022, "Elastic storage enables robustness of flapping wing dynamics," Bioinspiration Biomimetics **17**, 045003.

Cheer, A. Y. L., and M. A. R. Koehl, 1987, "Fluid flow through filtering appendages of insects," Math. Med. Biol. **4**, 185–199.

Cheng, B., X. Deng, and T. L. Hedrick, 2011, "The mechanics and control of pitching manoeuvres in a freely flying hawkmoth (*Manduca sexta*)," J. Exp. Biol. **214**, 4092.

Cheng, B., and X. Y. Deng, 2011, "Translational and rotational damping of flapping flight and its dynamics and stability at hovering," IEEE Trans. Rob. **27**, 849.

Cheng, X., and M. Sun, 2018, "Very small insects use novel wing flapping and drag principle to generate the weight-supporting vertical force," J. Fluid Mech. **855**, 646.

Cheng, X., and M. Sun, 2019, "Revisiting the clap-and-fling mechanism in small wasp *Encarsia formosa* using quantitative measurements of the wing motion," Phys. Fluids **31**, 101903.

Cheng, X., and M. Sun, 2021, "Wing kinematics and aerodynamic forces in miniature insect *Encarsia formosa* in forward flight," Phys. Fluids **33**, 021905.

Dickinson, M. H., F. O. Lehman, and S. P. Sane, 1999, "Wing rotation and the aerodynamic basis of insect flight," Science **284**, 1954.

Du, G., and M. Sun, 2010, "Effects of wing deformation on aerodynamic forces in hovering hoverflies," J. Exp. Biol. **213**, 2273.

Dudley, R., 2000, *The Biomechanics of Insect Flight: Form, Function, Evolution* (Princeton University Press, Princeton, NJ).

Dudley, R., and C. P. Ellington, 1990a, "Mechanics of forward flight in bumblebees. I. Kinematics and morphology," J. Exp. Biol. **148**, 19–52.

Dudley, R., and C. P. Ellington, 1990b, "Mechanics of forward flight in bumblebees. II. Quasi-steady lift and power requirements," J. Exp. Biol. **148**, 53.

Ellington, C. P., 1984a, "The aerodynamics of hovering insect flight. I. The quasi-steady analysis," Phil. Trans. R. Soc. B **305**, 1–15.

Ellington, C. P., 1984b, "The aerodynamics of hovering insect flight. II. Morphological parameters," Phil. Trans. R. Soc. B **305**, 17–40.

Ellington, C. P., 1984c, "The aerodynamics of hovering insect flight. III. Kinematics," Phil. Trans. R. Soc. B **305**, 41–78.

Ellington, C. P., 1984d, "The aerodynamics of hovering insect flight. IV. Aerodynamic mechanisms," Phil. Trans. R. Soc. B **305**, 79–113.

Ellington, C. P., C. van den Berg, A. P. Willmott, and A. L. R. Thomas, 1996, "Leading edge vortices in insect flight," Nature (London) **384**, 626.

Farisenkov, S. E., D. Kolomenskiy, P. N. Petrov, T. Engels, N. A. Lapina, F. O. Lehmann, R. Onishi, H. Liu, and A. A. Polilov, 2022, "Novel flight style and light wings boost flight performance of tiny beetles," Nature (London) **602**, 96.

Farisenkov, S. E., N. A. Lapina, P. N. Petrov, and A. A. Polilov, 2020, "Extraordinary flight performance of the smallest beetles," Proc. Natl. Acad. Sci. U.S.A. **117**, 24643.

Fry, S. N., R. Sayaman, and M. H. Dickinson, 2005, "The aerodynamics of hovering flight in *Drosophila*," J. Exp. Biol. **208**, 2303–2318.

Gao, N., H. Aono, and H. Liu, 2011, "Perturbation analysis of 6DoF flight dynamics and passive dynamic stability of hovering fruit fly *Drosophila melanogaster*," J. Theor. Biol. **270**, 98.

Hao, J. J., J. H. Wu, and Y. L. Zhang, 2019, "Aerodynamic performance of a passive pitching model on bionic flapping wing micro air vehicles," Appl. Bionics Biomech. 1504310.

Haselsteiner, A. F., C. Gilbert, and Z. J. Wang, 2014, "Tiger beetles pursue prey using a proportional control law with a delay of one half-stride," J. R. Soc. Interface **11**, 20140216.

Horridge, G. A., 1956, "The flight of very small insects," Nature (London) **178**, 1334.

Huber, J. T., and J. S. Noyes, 2013, "A new genus and species of fairyfly, *Tinkerbella nana* (*Hymenoptera*, *Mymaridae*), with comments on its sister genus *Kikiki*, and discussion on small size limits in arthropods," J. Hymenopt. Res. **32**, 17.

Ishihara, D., 2018, "Role of fluid-structure interaction in generating the characteristic tip path of a flapping flexible wing," Phys. Rev. E **98**, 032411.

Jiang, Y. G., *et al.*, 2022, "Bristled-wing design of materials, microstructures, and aerodynamics enables flapping flight in tiny wasps," iScience **25**, 103692.

Jones, S. K., R. Laurenza, T. L. Hedrick, B. E. Griffith, and L. A. Miller, 2015, "Lift versus drag based mechanisms for vertical force production in the smallest flying insects," J. Theor. Biol. **384**, 105.

Jones, S. K., Y. J. J. Yun, T. L. Hedrick, B. E. Griffith, and L. A. Miller, 2016, "Bristles reduce the force required to 'fling' wings apart in the smallest insects," J. Exp. Biol. **219**, 3759.

Kasoju, V. T., and A. Santhanakrishnan, 2021, "Aerodynamic interaction of bristled wing pairs in fling," Phys. Fluids **33**, 031901.

Kolomenskiy, D., S. Farisenkov, T. Engels, N. Lapina, P. Petrov, F. O. Lehmann, R. Onishi, H. Liu, and A. Polilov, 2020, "Aerodynamic performance of a bristled wing of a very small insect," Exp. Fluids **61**, 194.

Lee, S. H., M. Lee, and D. Kim, 2020, "Optimal configuration of a two-dimensional bristled wing," J. Fluid Mech. **888**, A23.

Lewis, T., 1973, *Thrips* (Academic Press, New York).

Liang, B., and M. Sun, 2013, "Nonlinear flight dynamics and stability of hovering model insects," J. R. Soc. Interface **10**, 20130269.

Liu, H., and H. Aono, 2009, "Size effects on insect hovering aerodynamics: An integrated computation study," Bioinspiration Biomimetics **4**, 015002.

Liu, H., and K. Kawachi, 1998, "A numerical study of insect flight," J. Comput. Phys. **146**, 124.

Liu, W. J., and M. Sun, 2023, "Rarefaction effect on the aerodynamics of bristled wings in miniature insects," Phys. Fluids **35**, 051901.

Liu, Y., and M. Sun, 2008, "Wing kinematics measurement and aerodynamics of hovering drone-flies," J. Exp. Biol. **211**, 2014.

Lyu, Y. Z., and M. Sun, 2021, "Power requirements for the hovering flight of insects with different sizes," J. Insect Physiol. **134**, 104293.

Lyu, Y. Z., and M. Sun, 2022, "Dynamic stability in hovering flight of insects with different sizes," Phys. Rev. E **105**, 054403.

Lyu, Y. Z., H. J. Zhu, and M. Sun, 2019a, "Aerodynamic forces and vortical structures of a flapping wing at very low Reynolds numbers," Phys. Fluids **31**, 041901.

Lyu, Y. Z., H. J. Zhu, and M. Sun, 2019b, "Flapping-mode changes and aerodynamic mechanisms in miniature insects," Phys. Rev. E **99**, 012419.

Maxworthy, T., 1979, "Experiments on the Weis-Fogh mechanism of lift generation by insects in hovering flight. Part I. Dynamics of the fling," J. Fluid Mech. **93**, 47.

Miller, L. A., and C. S. Peskin, 2004, "When vortices stick: An aerodynamic transition in tiny insect flight," J. Exp. Biol. **207**, 3073.

Miller, L. A., and C. S. Peskin, 2005, "A computational fluid dynamics of 'clap and fling' in the smallest insects," J. Exp. Biol. **208**, 195.

Miller, L. A., and C. S. Peskin, 2009, "Flexible clap and fling in tiny insect flight," J. Exp. Biol. **212**, 3076.

Nakata, T., and H. Liu, 2012a, "A fluid-structure interaction model of insect flight with flexible wings," J. Comput. Phys. **231**, 1822–1847.

Nakata, T., and H. Liu, 2012b, "Aerodynamic performance of a hovering hawkmoth with flexible wings: A computational approach," Proc. R. Soc. B **279**, 722.

Norberg, R. A., 1975, "Hovering flight of the dragonfly *Aeschna juncea L.*, kinematics and aerodynamics," in *Swimming and Flying in Nature*, edited by T. Y. Wu, C. J. Brokaw, and C. Brennen) (Plenum Press, New York), pp. 763–781.

Polilov, A. A., 2005, "Anatomy of the feather-winged beetles *Acrotrichis montandoni* and *Ptilium myrmecophilum* (*Coleoptera*, *Ptiliidae*)," Entomol. Rev. **85**, 467, http://www.entomology.narod.ru/archiv_text/polilov/polilov_2005_translated_anatomy_of_ptiliidae.pdf.

Polilov, A. A., 2015, "Small is beautiful: Features of the smallest insects and limits to miniaturization," Annu. Rev. Entomol. **60**, 103.

Richter, M., and M. J. Patil, 2010, "Influence of wing flexibility on the stability of flapping flight," AIAA Report No. 2010–7631.

Ristroph, L., A. J. Bergou, G. Ristroph, K. Coumes, G. J. Berman, J. Guckenheimer, Z. J. Wang, and I. Cohen, 2010, "Discovering the flight auto-stabilizer of fruit flies by inducing aerial stumbles," Proc. Natl. Acad. Sci. U.S.A. **107**, 4820.

Ristroph, L., G. Ristroph, S. Morozova, A. J. Bergou, S. Chang, J. Guckenheimer, Z. J. Wang, and I. Cohen, 2013, "Active and passive stabilization of body pitch in insect flight," J. R. Soc. Interface **10**, 20130237.

Sane, S. P., 2003, "The aerodynamics of insect flight," J. Exp. Biol. **206**, 4192.

Santhanakrishnan, A., A. K. Robinson, S. Jones, A. A. Low, S. Gadi, T. L. Hedrick, and L. A. Miller, 2014, "Clap and fling mechanism with interacting porous wings in tiny insect flight," J. Exp. Biol. **217**, 3898.

Seale, M., C. Cummins, I. M. Viola, E. Mastropaolo, and N. Nakayama, 2018, "Design principles of hair-like structures as biological machines," J. R. Soc. Interface **15**, 20180206.

Shelley, M., and J. Zhang, 2011, "Flapping and bending bodies interacting with fluid flows," Annu. Rev. Fluid Mech. **43**, 449.

Shyy, W., H. Aono, S. K. Chimakurthi, P. Trizila, C. K. Kang, C. E. S. Cesink, and H. Liu, 2010, "Recent progress in flapping wing aerodynamics and aeroelasticity," Prog. Aerosp. Sci. **46**, 284.

Sun, M., and G. Du, 2003, "Lift and power requirements of hovering insect flight," Acta Mech. Sin. **19**, 458–469.

Sun, M., and S. L. Lan, 2004, "A computational study of the aerodynamic forces and power requirements of dragonfly (*Aeschna juncea*) hovering," J. Exp. Biol. **207**, 1887–1901.

Sun, M., and J. Tang, 2002a, "Unsteady aerodynamic force generation by a model fruit-fly wing," J. Exp. Biol. **205**, 55.

Sun, M., and J. Tang, 2002b, "Lift and power requirements of hovering flight in *Drosophila virilis*," J. Exp. Biol. **205**, 2413.

Sun, M., and Y. Xiong, 2005, "Dynamic flight stability of a hovering bumblebee," J. Exp. Biol. **208**, 447.

Sun, M., and X. Yu, 2006, "Aerodynamic force generation in hovering flight in a tiny insect," AIAA J. **44**, 1532.

Sunada, S., H. Takashima, T. Hattori, K. Yasuda, and K. Kawachi, 2002, "Fluid-dynamic characteristics of a bristled wing," J. Exp. Biol. **205**, 2737.

Taha, H. E., M. Kiani, T. L. Hedrick, and J. S. M. Greeter, 2020, "Vibrational control: A hidden stabilization mechanism in insect flight," Sci. Robot. **5**, eabb1502.

Taylor, G. K., and A. L. R. Thomas, 2003, "Dynamic flight stability in the desert locust *Schistocerca gregaria*," J. Exp. Biol. **206**, 2803.

Umemura, A., 1982, "Matched-asymptotic analysis of low-Reynolds number flow past two equal circular cylinders," J. Fluid Mech. **121**, 345–363.

Walker, S. M., A. L. R. Thomas, and G. K. Taylor, 2010, "Deformable wing kinematics in free-flying hoverflies," J. R. Soc. Interface **7**, 131.

Wang, Z. J., 2004, "The role of drag in insect hovering," J. Exp. Biol. **207**, 4147–4155.

Wang, Z. J., 2005, "Dissecting insect flight," Annu. Rev. Fluid Mech. **37**, 183.

Wang, Z. J., J. M. Birch, and M. H. Dickinson, 2004, "Unsteady forces and flows in low Reynolds number hovering flight: Two-dimensional computations vs robotic wing experiments," J. Exp. Biol. **207**, 449.

Wang, Z. J., J. Melfi, Jr., and A. Leonardo, 2022, "Recovery mechanisms in the dragonfly righting reflex," Science **376**, 754.

Weihs, D., and E. Barta, 2008, "Comb-wings for flapping flight at extremely low Reynolds numbers," AIAA J. **46**, 285.

Weis-Fogh, T., 1973, "Quick estimates of flight fitness in hovering animals, including novel mechanisms for lift production," J. Exp. Biol. **59**, 169.

Windsor, S. P., R. J. Bomphrey, and G. K. Taylor, 2014, "Vision-based flight control in the hawkmoth *Hyles lineata*," J. R. Soc. Interface **11**, 20130921.

Wu, J. H., and M. Sun, 2012, "Floquet stability analysis of the longitudinal dynamics of two hovering model insects," J. R. Soc. Interface **9**, 2033–2046.

Wu, Y. K., Y. P. Liu, and M. Sun, 2021, "Unsteady aerodynamics of a model bristled wing in rapid acceleration motion," Phys. Fluids **33**, 111902.

Young, J., S. M. Walker, R. J. Bomphrey, G. K. Taylor, and A. L. R. Thomas, 2009, "Details of insect wing design and deformation enhance aerodynamic function and flight efficiency," Science **325**, 1549.

Zhu, H. J., and Sun, 2017, "Unsteady aerodynamic force mechanisms of a hoverfly hovering with a short stroke-amplitude," Phys. Fluids **29**, 081901.